

Optimizing Dynamic Predictions from Joint Models using Super Learning

Dimitris Rizopoulos^{1,2,*} and Jeremy M.G. Taylor³

¹Department of Biostatistics, Erasmus University Medical Center, the Netherlands

²Department of Epidemiology, Erasmus University Medical Center, the Netherlands

³Department of Biostatistics, University of Michigan, Ann Arbor, USA

Abstract

Joint models for longitudinal and time-to-event data are often employed to calculate dynamic individualized predictions used in numerous applications of precision medicine. Two components of joint models that influence the accuracy of these predictions are the shape of the longitudinal trajectories and the functional form linking the longitudinal outcome history to the hazard of the event. Finding a single well-specified model that produces accurate predictions for all subjects and follow-up times can be challenging, especially when considering multiple longitudinal outcomes. In this work, we use the concept of super learning and avoid selecting a single model. In particular, we specify a weighted combination of the dynamic predictions calculated from a library of joint models with different specifications. The weights are selected to optimize a predictive accuracy metric using V-fold cross-validation. We use as predictive accuracy measures the expected quadratic prediction error and the expected predictive cross-entropy. In a simulation study, we found that the super learning approach produces results very similar to the Oracle model, which was the model with the best performance in the test datasets. All proposed methodology is implemented in the freely available R package **JMbayes2**.

Keywords: Brier score, Cross-entropy, Precision medicine, Prognostic models, Survival analysis, Time-varying covariates.

*Correspondence at: Department of Biostatistics, Erasmus University Medical Center, PO Box 2040, 3000 CA Rotterdam, the Netherlands. E-mail address: d.rizopoulos@erasmusmc.nl.

1 Introduction

Joint models for longitudinal and time-to-event data have been established as a versatile tool for calculating dynamic predictions for longitudinal and survival outcomes (Taylor et al. 2005; Rizopoulos 2011; Taylor et al. 2013). The advantageous feature of these predictions is that they are updated over time as extra information becomes available. As a result, they have found numerous applications in precision medicine, including cancer and cardiovascular diseases.

The motivation for our research comes from prostate cancer patients who, after diagnosis, underwent surgical removal of the prostate gland (radical prostatectomy). The treating physicians closely monitor the prostate-specific antigen (PSA) levels of these patients to determine the risk of recurrence and metastasis. Increasing PSA values suggest the cancer may be regrowing, although it is generally not yet detectable on imaging. After the initial surgery, PSA levels drop to near zero; however, PSA may rise again for some patients, leading the treating physicians to recommend salvage therapy to reduce their risk of metastasis. After salvage therapy, PSA levels nearly always drop, sometimes substantially, but typically rise again if metastasis is going to occur.

Optimizing the accuracy of dynamic predictions from joint models is a difficult task, especially when multiple longitudinal outcomes are considered. In particular, previous research has shown that two aspects are important (Ferrer et al. 2019). First, the time trend specification in the mixed-effects models, and second, the functional forms that specify how the longitudinal histories are linked to the hazard of the event. Previous applications of joint models have considered a single model for obtaining dynamic predictions. However, due to the aforementioned complexities, finding a well-specified model can be challenging, especially when multiple longitudinal outcomes are considered. Moreover, due to the dynamic nature of these predictions, different models may provide different levels of predictive accuracy at different follow-up times.

Standard approaches for model selection within the Bayesian framework include information criteria and (pseudo-) Bayes factors. However, these methods provide an overall assessment of a model’s fit. In contrast, we are particularly interested in the model that best predicts future events given that subject i was event-free up to time point t , i.e., the conditional cumulative risk probabilities. Moreover, in practice, it will seldom be the case that a single model provides the most accurate predictions for all subjects and time points. In this work, we consider multiple joint models instead and combine the dynamic predictions from these models to optimize the predictive accuracy. Under the Bayesian paradigm, an established method to combine quantities from different statistical models is Bayesian model averaging (BMA) (Hoeting et al. 1999). Rizopoulos et al. (2014) have previously used BMA to combine dynamic predictions from a library of joint models. Even though BMA enjoys several optimality properties, it also has some disadvantages. First, it requires calculating the marginal likelihood under each posited model, which is a computationally demanding task. Second, the BMA weights are not explicitly designed to optimize the accuracy of predictions, and it is unclear if they appropriately account for over-fitting. Finally, the weights are defined using the posterior distribution of each model given the data. As a result, even though the competing models may not differ much in their posterior densities (considering the likelihood’s magnitude), the differences are large enough that often, one model dominates the weights over the others.

We will use the concept of super learning (SL) to overcome these issues (Breiman 1996; van der Laan et al. 2006, 2007; Naimi and Balzer 2018; Phillips et al. 2023). SL is an ensemble method that allows researchers to combine several different prediction algorithms into one. It uses V -fold cross-validation to build the optimally weighted combination of predictions from a library of candidate algorithms. Optimality is defined by a user-specified objective function, such as minimizing the mean squared error or maximizing the area under the receiver operating characteristic curve. Here we will consider a library of joint models with different specifications and present appropriate objective functions for optimizing the

accuracy of dynamic predictions. In particular, we focus on different formulations of the time effect for the longitudinal outcome and different functional forms to link this outcome with the event process. We measure the dynamic predictions' accuracy using the expected Brier score and the expected predictive cross-entropy and show how these are formulated under the SL framework.

The rest of the paper is organized as follows: Section 2 presents the joint models' framework. Section 3 introduces the Super Learning technique in the context of joint models and dynamic predictions and presents the two accuracy measures for combining the predictions from different models. Section 4 employs SL in the context of the University of Michigan Prostatectomy Data, and Section 5 shows the results of a simulation study that evaluates the performance of SL. Finally, Section 6 closes the paper with a discussion.

2 Joint Modeling Framework

2.1 Joint Models

In this section, we present a general definition of the joint modeling framework for longitudinal and time-to-event data (Rizopoulos 2012). Let $\mathcal{D}_n = \{T_i, \delta_i, \mathbf{y}_i; i = 1, \dots, n\}$ denote a sample from the target population, where T_i^* denotes the true event time for the i -th subject, C_i the censoring time, $T_i = \min(T_i^*, C_i)$ the corresponding observed event time, and $\delta_i = \mathbb{I}(T_i^* \leq C_i)$ the event indicator, with $\mathbb{I}(\cdot)$ being the indicator function that takes the value 1 when $T_i^* \leq C_i$, and 0 otherwise. In addition, we let \mathbf{y}_i denote the $n_i \times 1$ longitudinal response vector for the i -th subject, with element y_{il} denoting the value of the longitudinal outcome taken at time point t_{il} , $l = 1, \dots, n_i$.

To accommodate different types of longitudinal responses in a unified framework, we postulate that the response vector \mathbf{y}_i conditional on the vector of unobserved random effects \mathbf{b}_i has a distribution \mathcal{F}_ψ parameterized by the vector ψ . This more general formulation

allows for distributions not covered by the exponential family. The mean of the distribution of the longitudinal outcome conditional on the random effects has the form

$$g[E\{y_i(t) \mid \mathbf{b}_i\}] = \eta_i(t) = \mathbf{x}_i^\top(t)\boldsymbol{\beta} + \mathbf{z}_i^\top(t)\mathbf{b}_i, \quad (1)$$

where $g(\cdot)$ denotes a known one-to-one monotonic link function, and $y_i(t)$ denotes the value of the longitudinal outcome for the i -th subject at time point t , $\mathbf{x}_i(t)$ and $\mathbf{z}_i(t)$ denote the time-dependent design vectors for the fixed-effects $\boldsymbol{\beta}$ and for the random effects \mathbf{b}_i , respectively. We let ϕ denote the scale parameter of \mathcal{F}_ψ , i.e., $\boldsymbol{\psi}^\top = (\boldsymbol{\beta}^\top, \phi)$. The random effects are assumed to follow a multivariate normal distribution with mean zero and variance-covariance matrix \mathbf{D} . For the survival process, we assume that the risk of an event depends on a function of the subject-specific linear predictor $\eta_i(t)$ and the random effects. More specifically, we have

$$\begin{aligned} h_i\{t \mid \mathcal{H}_i(t), \mathbf{w}_i\} &= \lim_{s \rightarrow 0} \Pr\{t \leq T_i^* < t + s \mid T_i^* \geq t, \mathcal{H}_i(t), \mathbf{w}_i\}/s \\ &= h_0(t) \exp[\boldsymbol{\gamma}^\top \mathbf{w}_i + f\{\eta_i(t), \mathbf{b}_i, \boldsymbol{\alpha}\}], \quad t > 0, \end{aligned} \quad (2)$$

where $\mathcal{H}_i(t) = \{\eta_i(s), 0 \leq s < t\}$ denotes the history of the underlying longitudinal process up to t , $h_0(\cdot)$ denotes the baseline hazard function, \mathbf{w}_i is a vector of baseline covariates with corresponding regression coefficients $\boldsymbol{\gamma}$. Finally, the baseline hazard function $h_0(\cdot)$ is modeled flexibly using a B-splines approach, i.e.,

$$\log h_0(t) = \gamma_{h_0,0} + \sum_{p=1}^P \gamma_{h_0,p} B_p(t, \boldsymbol{\lambda}), \quad (3)$$

where $B_p(t, \mathbf{v})$ denotes the p -th basis function of a B-spline with knots $\lambda_1, \dots, \lambda_P$ and $\boldsymbol{\gamma}_{h_0}$ the vector of spline coefficients.

The function $f(\cdot)$, parameterized by vector $\boldsymbol{\alpha}$, specifies which components/features of the

longitudinal outcome process are included in the linear predictor of the relative risk model. Some examples previously considered in the literature are:

$$f\{\mathcal{H}_i(t), \mathbf{b}_i, \boldsymbol{\alpha}\} = \begin{cases} \alpha\eta_i(t), \\ \alpha\eta'_i(t), \text{ with } \eta'_i(t) = \frac{d\eta_i(t)}{dt}, \\ \alpha\eta''_i(t), \text{ with } \eta''_i(t) = \frac{d^2\eta_i(t)}{dt^2}, \\ \alpha\frac{1}{v} \int_{t-v}^t \eta_i(s) ds, \quad 0 < v \leq t, \\ \boldsymbol{\alpha}^\top \mathbf{b}_i. \end{cases}$$

These formulations of $f(\cdot)$ postulate that the hazard of an event at time t is associated with the underlying level of the biomarker at the same time point, the slope/velocity of the biomarker at t , the acceleration of the biomarker at t , the average biomarker level in the period $(t - v, t)$, or the random effects alone. Combinations of these functional forms and their interactions with baseline covariates are also often considered.

2.2 Bayesian Estimation

We let $\boldsymbol{\theta}^\top = (\boldsymbol{\beta}^\top, \phi, \boldsymbol{\gamma}_{h_0}^\top, \boldsymbol{\gamma}^\top, \boldsymbol{\alpha}^\top, \text{vech}(\mathbf{D})^\top, \tau)$ to denote the vector of all model parameters, where $\text{vech}(\mathbf{D})$ denotes the unique elements of the variance-covariance matrix \mathbf{D} . We proceed under the Bayesian paradigm and draw inferences using the joint posterior distribution $\{\boldsymbol{\theta}, \mathbf{b} \mid \mathbf{Y}, \mathbf{T}, \boldsymbol{\delta}\}$, where \mathbf{Y} , \mathbf{T} , and $\boldsymbol{\delta}$ denote outcome vectors for all n subjects. We use standard priors for $\boldsymbol{\theta}$, i.e., normal priors for all regression coefficients $(\boldsymbol{\beta}, \boldsymbol{\gamma}, \boldsymbol{\gamma}_{h_0}, \boldsymbol{\alpha})$, inverse-Gamma priors for ϕ and the diagonal elements of \mathbf{D} , and the LKJ prior for the correlation matrix of the random effects (Lewandowski et al. 2009). To ensure smoothness of the baseline hazard function $h_0(t)$, we postulate a ‘penalized’ prior distribution for the regression coefficients $\boldsymbol{\gamma}_{h_0}$:

$$p(\boldsymbol{\gamma}_{h_0} \mid \tau) \propto \tau^{\rho(K)/2} \exp\left(-\frac{\tau}{2} \boldsymbol{\gamma}_{h_0}^\top \mathbf{K} \boldsymbol{\gamma}_{h_0}\right),$$

where τ is the smoothing parameter that takes a Gamma(5, 0.05) hyper-prior in order to ensure a proper posterior for γ_{h_0} , $\mathbf{K} = \Delta_r^\top \Delta_r$, where Δ_r denotes r -th difference penalty matrix, and $\rho(\mathbf{K})$ denotes the rank of \mathbf{K} . We should note here that τ is also included in $\boldsymbol{\theta}$.

We use a Markov chain Monte Carlo (MCMC) approach to obtain samples from the posterior distribution for all model parameters and the random effects. This algorithm is implemented in the freely available R package **JMbayes2** (Rizopoulos et al. 2023) that we used to fit the model.

3 Optimizing Predictions via Super Learning

3.1 Model Weights

The basic idea behind super learning is to derive model weights that optimize the cross-validated predictions. More specifically, we let $\mathcal{L} = \{M_1, \dots, M_L\}$ denote a library with L models. There are no restrictions to the models included in this library, and actually, it is recommended to consider a wide range of possible models. Among others, these joint models differ in the specification of the time trend in the longitudinal submodels (e.g., linear or nonlinear trajectories), the functional form for the longitudinal outcome in the event submodel, and the functional form of the other covariates (e.g., interactions and nonlinear terms) in both submodels.

We split the original dataset \mathcal{D}_n in V folds. The choice of V will depend on the size and number of events in \mathcal{D}_n (Phillips et al. 2023). In particular, for each fold, we need to have a sufficient number of events to robustly quantify the predictive performance. Using the cross-validation method, we fit the L models in the combined $v - 1$ folds, and we will calculate predictions for the v -th fold we left outside. Due to the dynamic nature of the predictions, we want to derive optimal weights at different follow-up times. More specifically, we consider the sequence of time points t_1, \dots, t_Q . The number and placing of these time points should

again consider the available event information in \mathcal{D}_n . For example, we should have at least 10-15 events per time interval (t_{q-1}, t_q) , with $q = 1, \dots, Q$, and $t_0 = 0$.

For any $t_q \in \{t_1, \dots, t_Q\}$, we define $\mathcal{R}(t_q, v)$ to denote the subjects at risk at time t_q that belong to the v -th fold. For all subjects in $\mathcal{R}(t_q, v)$, we calculate the cross-validated predictions (conditioning on the covariates \mathbf{w}_i , \mathbf{x}_i and \mathbf{z}_i is assumed in the following expressions but is dropped to simplify notation),

$$\hat{\pi}_i^{(v)}(t_q + \Delta t \mid t_q, M_l) = \Pr\{T_i^* < t_q + \Delta t \mid T_i^* > t_q, \mathcal{H}_i(t), M_l, \mathcal{D}_n^{(-v)}\}.$$

These predictions are calculated based on model M_l in library \mathcal{L} that was fitted in the dataset $\mathcal{D}_n^{(-v)}$ that excludes the subjects in the v -th fold. The calculation is based on a Monte Carlo approach (Rizopoulos 2011). We define $\hat{\pi}_i^v(t_q + \Delta t \mid t_q)$ to denote the convex combination of the L predictions, i.e.,

$$\hat{\pi}_i^v(t_q + \Delta t \mid t_q) = \sum_{l=1}^L \varpi_l(t_q) \hat{\pi}_i^{(v)}(t_q + \Delta t \mid t_q, M_l), \quad \text{for all } v \in 1, \dots, V, \quad (4)$$

with $\varpi_l(t_q) > 0$, for $l = 1, \dots, L$, and $\sum_l \varpi_l(t_q) = 1$. Note that the weights $\varpi_l(\cdot)$ are time-varying, i.e., at different follow-up times, different combinations of the L models may yield more accurate predictions. The weighted combination of the predictions from the L models is typically called the ensemble super learner (eSL). The model with the best cross-validated prediction metric is called the discrete super learner (dSL). Most often, but not always, this is the model with the largest weight $\varpi_l(\cdot)$.

3.2 Measuring Predictive Performance

For the ensemble super learner and for any time t , we will select the weights $\{\varpi_l(t); l = 1, \dots, L\}$ that optimize the predictive performance of the combined cross-validated predictions. We will employ the framework of proper scoring rules to achieve that. A scoring rule

$\mathcal{S}\{\pi_i(u | t), \mathbb{I}(t < T_i^* < u)\}$ is called proper if the true distribution achieves the optimal expected score, i.e., in our case if

$$E\left[\mathcal{S}\{\pi_i^{true}(u | t), \mathbb{I}(t < T_i^* < u)\}\right] \leq E\left[\mathcal{S}\{\hat{\pi}_i(u | t), \mathbb{I}(t < T_i^* < u)\}\right], \quad u > t,$$

where $\pi_i^{true}(u | t)$ denotes the conditional risk probabilities under the true model, and $\hat{\pi}_i(u | t)$ is an estimate of $\pi_i^{true}(u | t)$. The expectation is taken with respect to the conditional density of the survival outcome under the true model $\{T_i^* | T_i^* > t, \mathcal{Y}_i(t)\}$, with $\mathcal{Y}_i(t) = \{y_i(t_{il}); 0 \leq t_{il} \leq t, l = 1, \dots, n_i\}$, and the scoring rule $\mathcal{S}(\cdot, \cdot)$ is defined such that a lower score indicates better accuracy.

The Brier score is a proper scoring rule that combines discrimination and calibration to measure overall predictive performance. In particular, at follow-up time t and for a medically-relevant time window Δt , we define the Brier score as

$$\text{BS}(t + \Delta t, t) = E\left[\left\{\mathbb{I}(T_i^* \leq t + \Delta t) - \tilde{\pi}_i^v(t + \Delta t | t)\right\}^2 \mid T_i^* > t\right].$$

The Brier score evaluates the predictive accuracy at time $t + \Delta t$. To summarize the predictive accuracy in the interval $(t, t + \Delta t]$, we can use the integrated Brier score,

$$\text{IBS}(t + \Delta t, t) = \frac{1}{\Delta t} \int_t^{t+\Delta t} \text{BS}(s, t) ds.$$

In practice, this integral does not have a closed-form solution and needs to be approximated numerically. In our examples, we use Simpson's rule to approximate it, i.e.,

$$\text{IBS}(t + \Delta t, t) \approx \frac{2}{3}\text{BS}(t + 0.5\Delta t, t) + \frac{1}{6}\text{BS}(t + \Delta t, t),$$

where we have dropped the first term of the approximation because $\text{BS}(t, t) = 0$.

To estimate $\text{BS}(t + \Delta t, t)$, we need to appropriately account for patients who were censored

in the interval $(t, t + \Delta t]$. Two approaches to achieve this is using inverse probability of censoring weights (IPCW), and model-based weights. In the former approach, we only use the subjects who had an event before $t + \Delta t$, and the ones for whom we know that they survived up to $t + \Delta t$; patients censored in $(t, t + \Delta t]$ do not contribute, that is,

$$\widehat{\text{BS}}_{\text{IPCW}}(t + \Delta t, t) = \frac{1}{n_t} \sum_{i: T_i > t} \widehat{W}_i(t + \Delta t, t) \left\{ \mathbb{I}(T_i \leq t + \Delta t) - \hat{\pi}_i^v(t + \Delta t | t) \right\}^2,$$

where n_t denotes the number of subjects at risk at time t , and

$$\widehat{W}_i(t + \Delta t, t) = \frac{\mathbb{I}(t < T_i \leq t + \Delta t) \delta_i}{\widehat{G}(T_i | t)} + \frac{\mathbb{I}(T_i > t + \Delta t)}{\widehat{G}(t + \Delta t | t)} + 0 \cdot \mathbb{I}(t < T_i \leq t + \Delta t)(1 - \delta_i),$$

with $\widehat{G}(\cdot)$ denoting Kaplan-Meier estimate of the censoring distribution $\Pr(C_i > t)$.

The model-based approach uses all subjects at risk at time t , i.e.,

$$\begin{aligned} \widehat{\text{BS}}_{\text{model}}(t + \Delta t, t) &= \frac{1}{n_t} \sum_{i: T_i > t} \delta_i \mathbb{I}(T_i \leq t + \Delta t) \left\{ 1 - \hat{\pi}_i^v(t + \Delta t | t) \right\}^2 \\ &\quad + \mathbb{I}(T_i > t + \Delta t) \left\{ \hat{\pi}_i^v(t + \Delta t | t) \right\}^2 \\ &\quad + (1 - \delta_i) \mathbb{I}(T_i \leq t + \Delta t) \left[\hat{\pi}_i^v(t + \Delta t | T_i) \left\{ 1 - \hat{\pi}_i^v(t + \Delta t | t) \right\}^2 \right. \\ &\quad \left. + \left\{ 1 - \hat{\pi}_i^v(t + \Delta t | T_i) \right\} \left\{ \hat{\pi}_i^v(t + \Delta t | t) \right\}^2 \right]. \end{aligned}$$

Both approaches have their merits and flaws. The IPCW approach is model-free in the sense that there is no assumption about the correctness of the specification of the joint model used for computing $\hat{\pi}_i^{(v)}(t_q + \Delta t | t_q, M_l)$. On the other hand, it makes the strong assumption that censoring does not depend on covariates and, more importantly, on the history of the longitudinal biomarker $\mathcal{Y}_i(t)$. This assumption is crucial because the Brier score is a proper scoring rule only when it holds (Rindt et al. 2022). When an inaccurate assumption is made for the censoring weights, we may achieve an incorrect Brier score that is lower in value (i.e., better) than the Brier score under the true weights (Kvamme and

Borgan 2023). In the clinical and epidemiological contexts where joint models are applied, physicians may decide to remove patients from a study based on their previously observed longitudinal measurements. Moreover, it may also be the case that different physicians use in another way the longitudinal history to exclude patients, e.g., one physician may decide to use just the last observed value of the biomarker. In contrast, another may remove patients who showed a sudden increase/decrease in the biomarker in the last two measurements. In situations like this, specifying an appropriate model for the censoring process is challenging, and thus, the appealing features of the IPCW approach are lost.

The model-based weights approach does not require modeling the censoring process. In particular, it will provide valid estimates of the Brier score even when censoring depends in a complex manner on the longitudinal history. However, it requires that the joint model is well-specified, which, as argued in Section 1, is also a strong assumption. And when we compare two or more models, it is paradoxical that all of them will be correctly specified, leading to unfair comparisons between them. However, in the context we consider here, the disadvantage of the model-based approach is alleviated. This is because we are not interested in comparing between models but rather combining the predictions from these models to improve accuracy. That is, the weights for the censored subjects are not calculated from a single model but as a convex combination of the weights from the L models. In addition, as we will see later, the weights $\{\varpi_l(t); l = 1, \dots, L\}$ are derived from the cross-validated predictions that ensure that predictions from over-fitted models will be down-weighted.

As an alternative proper scoring rule in the interval $(t, t + \Delta t]$ we consider an adaptation of the expected predictive cross-entropy proposed by Commenges et al. (2012):

$$\text{EPCE}(t + \Delta t, t) = E \left\{ -\log \left[p\{T_i^* \mid t < T_i^* \leq t + \Delta t, \mathcal{Y}_i(t), \mathcal{D}_n\} \right] \right\},$$

where the expectation is taken with respect to $\{T_i^* \mid T_i^* > t, \mathcal{Y}_i(t)\}$ under the true model. An estimate of $\text{EPCE}(t + \Delta t, t)$ that accounts for censoring can be obtained using the sample

at hand,

$$\widehat{\text{EPCE}}(t + \Delta t, t) = \frac{1}{n_t} \sum_{i: T_i > t} -\log \left[p\{\tilde{T}_i, \tilde{\delta}_i \mid T_i > t, \mathcal{Y}_i(t), \mathcal{D}_n\} \right],$$

where $\tilde{T}_i = \min(T_i, t + \Delta t)$ and $\tilde{\delta}_i = \delta_i \mathbb{I}(t < T_i \leq t + \Delta t)$. The $\text{EPCE}(t + \Delta t, t)$ makes the same assumptions regarding censoring as the model-based weights for $\text{BS}(t + \Delta t, t)$; namely that $T_i^* \perp\!\!\!\perp C_i \mid \mathcal{Y}_i(t), \mathbf{w}_i$. However, because no model weights are required to account for censoring, it does not share the disadvantage of $\text{BS}(t + \Delta t, t)$ mentioned above. The disadvantage of the $\text{EPCE}(t + \Delta t, t)$ over the Brier score is interpretability. Namely, the Brier score estimates a well-defined parameter in the population, the mean squared distance between the observed and expected outcomes. The square root of the Brier score is thus the expected distance between the observed and predicted value on the probability scale. On the contrary, the value of the expected predictive cross-entropy does not have a simple interpretation.

To use the EPCE for obtaining the super-learning model-specific weights, we need to formulate it as a function of the dynamic predictions from a joint model. It is convenient to redefine $\pi_i(u \mid t, M_l)$ as the dynamic subject-specific survival probabilities, i.e.,

$$\pi_i(u \mid t, M_l) = \Pr\{T_i^* > u \mid T_i^* > t, \mathcal{Y}_i(t), \mathcal{D}_n, M_l\}, \quad u > t.$$

Then we write the conditional predictive log-likelihood as (conditioning on M_l is assumed but it is omitted from the following expressions for exposition):

$$\begin{aligned} \log \left[p\{\tilde{T}_i, \tilde{\delta}_i \mid T_i > t, \mathcal{Y}_i(t), \mathcal{D}_n\} \right] = \\ \tilde{\delta}_i \log[h_i\{\tilde{T}_i \mid \mathcal{Y}_i(t), \mathcal{D}_n\}] + \log \frac{\Pr\{T_i^* > \tilde{T}_i \mid \mathcal{Y}_i(t), \mathcal{D}_n\}}{\Pr\{T_i^* > t \mid \mathcal{Y}_i(t), \mathcal{D}_n\}}. \end{aligned}$$

The second term is $\log\{\pi_i(\tilde{T}_i | t)\}$. For the first term, we write the hazard function as

$$h_i\{\tilde{T}_i | \mathcal{Y}_i(t), \mathcal{D}_n\} = -\frac{\frac{d}{dt} \Pr\{T_i^* > t | \mathcal{Y}_i(t), \mathcal{D}_n\} \Big|_{t=\tilde{T}_i}}{\Pr\{T_i^* > \tilde{T}_i | \mathcal{Y}_i(t), \mathcal{D}_n\}},$$

and we approximate the derivative with a forward difference, i.e.,

$$\begin{aligned} h_i\{\tilde{T}_i | \mathcal{Y}_i(t), \mathcal{D}_n\} &\approx -\frac{\Pr\{T_i^* > \tilde{T}_i + \epsilon | \mathcal{Y}_i(t), \mathcal{D}_n\} - \Pr\{T_i^* > \tilde{T}_i | \mathcal{Y}_i(t), \mathcal{D}_n\}}{\epsilon \Pr\{T_i^* > \tilde{T}_i | \mathcal{Y}_i(t), \mathcal{D}_n\}} \\ &= \frac{1 - \pi_i(\tilde{T}_i + \epsilon | \tilde{T}_i)}{\epsilon}, \quad \epsilon \rightarrow 0. \end{aligned}$$

Combining these two terms, we get the final expression:

$$\begin{aligned} \widehat{\text{EPCE}}(t + \Delta t, t) &= \\ &-\frac{1}{n_t} \sum_{i:\tilde{T}_i > t} \tilde{\delta}_i [\log\{1 - \pi_i(\tilde{T}_i + \epsilon | \tilde{T}_i)\} - \log(\epsilon)] + \log\{\pi_i(\tilde{T}_i | t)\}. \end{aligned}$$

In practice, we can compute $\widehat{\text{EPCE}}(t + \Delta t, t)$ using a small value for ϵ , e.g., $\epsilon = 0.001$. Numerical experiments we performed showed that the EPCE values are minimally affected by the value of ϵ .

In our context, both $\text{BS}(t + \Delta t, t)$ and $\text{EPCE}(t + \Delta t, t)$ are calculated using the convex combination of the cross-validated predictions $\hat{\pi}_i^v(t + \Delta t | t)$. In particular, using the super-learning procedure, we obtain the weights $\hat{\varpi}_l(t)$ that minimize a proper scoring rule (in our case, either the $\text{BS}(t + \Delta t, t)$ or $\text{EPCE}(t + \Delta t, t)$) of the cross-validated predictions,

$$\hat{\varpi}_l(t) = \arg \min_{\varpi} \left[\sum_{v=1}^V \mathcal{S} \left\{ \sum_{l=1}^L \varpi_l \hat{\pi}_i^{(v)}(t + \Delta t | t, M_l), T_i, \delta_i \right\} \right],$$

under the constraints $\varpi_l(t) > 0$, for $l = 1, \dots, L$, and $\sum_l \varpi_l(t) = 1$. We can transform to an unconstrained optimization problem using the logistic transformation and use a general-purpose minimization algorithm (e.g., using functions `optim()` or `nlmnb()` in R).

The vignette Combined Dynamic Predictions via Super Learning (available at https://drizopoulos.github.io/JMbayes2/articles/Super_Learning.html) describes how the super learning procedure is implemented in package **JMbayes2**.

4 University of Michigan Prostatectomy Data Analysis

We return to our motivating University of Michigan Prostatectomy Data. This database includes 3634 PCa patients who underwent a radical prostatectomy during the period 1996–2013. Of those patients, 271 (15.6%) received salvage therapy, 102 (2.8%) developed metastasis, and 209 (5.8%) died without metastases. Of these 209 patients, 190 died before salvage therapy, and 19 died after. Since death due to prostate cancer is extremely rare without prior metastases, these deaths are considered due to other causes. Here we focus on metastasis. PSA levels have been routinely collected for these patients to monitor progression. There are a total of 24673 PSA measurements, with a median of six measurements per patient (IQR: six measurements). We aim to utilize the longitudinal PSA measurements and baseline information (Gleason score, T-stage of the tumors, age, race, comorbidities) to predict metastasis and aid the decision-making process of urologists.

In particular, we considered four versions of the linear mixed-effects model for the $\log(\text{PSA} + 1)$ longitudinal outcome. In the first model, we specified linear subject-specific time trends for $\log(\text{PSA} + 1)$ that change after the first salvage therapy. The second model considers the same specification as the previous model, but we additionally include the baseline covariates age at surgery, Charlson’s index, Gleason score, and baseline PSA. These covariates are allowed to have a different effect after salvage. The third model considers nonlinear subject-specific time trends before salvage and linear subject-specific time trends after salvage. The final fourth model has the same specification for the time trends as the third one, but we again include the same covariates as in the second model. Using each of these linear mixed models, we fitted three joint models with different specifications of the

hazard submodel for metastasis. In the first hazard model, we consider the current value of $\log(\text{PSA} + 1)$; in the second one, the current value and the velocity of $\log(\text{PSA} + 1)$; and in the third one, the mean $\log(\text{PSA} + 1)$ from the start of the follow-up. In each hazard model, we include the same covariates as the one mentioned in the second and fourth linear mixed models above. Hence, in total, we consider twelve joint models. The exact specification of these models is presented in the supplementary material.

We split the UMP data into five folds and fitted the twelve joint models holding out a fold each time. We calculated the cross-validated predictions from these models for the fold not used when fitting them. We aim to evaluate the predictive performance of the twelve models in two medically-relevant time intervals $(t, t + \Delta t]$, namely, $(4, 7]$ and $(6, 9]$. At follow-up year 4, 2514 patients are still at risk, and 28 patients with metastasis in the interval $(4, 7]$. At follow-up year 6, 1914 patients are still at risk, and 16 patients with metastasis in the interval $(6, 9]$. We use as predictive performance metrics the integrated Brier score and the expected predictive cross-entropy. We calculated these metrics for each model using its cross-validated predictions. We also obtained the super learning weights that combined the dynamic predictions from these models to optimize the two prediction metrics and calculated the two metrics using the weighted predictions. Tables 1 and 2 present the results. We observed that for both time intervals the differences between the integrated Brier score are small. However, in the $(6, 9]$ interval the IBE for the joint model with linear subject-specific time trends and the mean $\log(\text{PSA} + 1)$ functional form (with and without baseline covariates) is smaller than the other model specifications. This is also reflected in the corresponding model weights. In particular, the model weights for the IBE in the interval $(4, 7]$ are effectively equal for all models, but in the $(6, 9]$ interval, the joint model specification mentioned above dominates the weights distribution. The expected predictive cross-entropy seems more sensitive in quantifying differences in the predictive performance of the different models. This also results in smaller super learning estimates of the EPCE than in each of the twelve models, and for both time intervals. In the $(4, 7]$ interval the

Table 1: Integrated Brier Score (IBE) for the University of Michigan Prostatectomy Data under the twelve joint models, and their combination using super learning. Results are based on 5-fold cross-validation.

	$(t, t + \Delta t] = (4, 7]$		$(t, t + \Delta t] = (6, 9]$	
	IBE	weights	IBE	weights
SL	0.00639		0.00530	
linear-noCov-value	0.00627	0.08334	0.00538	0.00352
linear-noCov-slope	0.00631	0.08342	0.00546	0.00136
linear-noCov-mean	0.00649	0.08329	0.00530	0.31705
linear-Cov-value	0.00626	0.08344	0.00538	0.01732
linear-Cov-slope	0.00630	0.08342	0.00547	0.00124
linear-Cov-mean	0.00652	0.08327	0.00529	0.52883
nonlinear-noCov-value	0.00646	0.08331	0.00552	0.00009
nonlinear-noCov-slope	0.00644	0.08332	0.00558	0.00002
nonlinear-noCov-mean	0.00653	0.08327	0.00535	0.08450
nonlinear-Cov-value	0.00643	0.08332	0.00553	0.00008
nonlinear-Cov-slope	0.00643	0.08333	0.00552	0.00008
nonlinear-Cov-mean	0.00654	0.08326	0.00537	0.04589

nonlinear joint models with no covariates and the slope and mean functional form dominate the weights. In the $(6, 9]$ interval the weights are distributed among almost all models.

5 Simulation Study

5.1 Objectives and Design

We have performed a simulation study to evaluate the performance of the super learning algorithm in the joint modeling context. For the longitudinal submodel, we consider two settings for the shape of the subject-specific longitudinal trajectories, namely, linear and nonlinear. For the survival submodel, we consider three settings for the functional forms, namely, the underlying value, the velocity, and the average longitudinal outcome level in the period $(0, t)$. Hence, in total, we consider six data-generating models. We simulated training and testing data under three scenarios; in Scenario I, each simulated training dataset contains 125 subjects from each of the six models ($n = 750$); in Scenario II, each simulated training dataset contains 450 subjects from the nonlinear model using the velocity functional form,

Table 2: Expected predictive cross-entropy (EPCE) for the University of Michigan Prostatectomy Data under the twelve joint models, and their combination using super learning. Results are based on 5-fold cross-validation.

	$(t, t + \Delta t] = (4, 7]$		$(t, t + \Delta t] = (6, 9]$	
	EPCE	weights	EPCE	weights
SL	0.07208		0.05166	
linear-noCov-value	0.07347	0.00026	0.05543	0.03259
linear-noCov-slope	0.07299	0.00004	0.05471	0.15417
linear-noCov-mean	0.07476	0.00235	0.05365	0.01329
linear-Cov-value	0.07338	0.00000	0.05506	0.02167
linear-Cov-slope	0.07298	0.00006	0.05455	0.09639
linear-Cov-mean	0.07484	0.00274	0.05353	0.02836
nonlinear-noCov-value	0.07324	0.00000	0.05376	0.01562
nonlinear-noCov-slope	0.07242	0.79539	0.05436	0.00317
nonlinear-noCov-mean	0.07457	0.18346	0.05303	0.02524
nonlinear-Cov-value	0.07316	0.00000	0.05337	0.10840
nonlinear-Cov-slope	0.07265	0.00121	0.05283	0.08131
nonlinear-Cov-mean	0.07454	0.01448	0.05284	0.41979

and 60 subjects from each of the five other models ($n = 750$). Scenarios III has the same settings as Scenario I, but the censoring mechanism is informative. That is, the probability of withdrawing a subject from the training dataset depends on their longitudinal outcome. The testing datasets under all scenarios have the same specification as the corresponding training datasets. The censoring was for all scenarios, on average, 45%. The parameter values and the other simulation settings we used can be found in the supplementary material. For each scenario, we simulated 250 datasets.

For each simulated training dataset, we implemented three-fold cross-validation, fitting the six models described above. The cross-validated predictions from each model were used to estimate the model weights to optimize predictive performance via the super learning procedure. The discrete super learner was also compared with the ensemble super learner. As predictive performance metrics, we used the integrated Brier score and the EPCE in two time intervals $(t, t + \Delta t]$, namely, $(16, 18]$ and $(19, 21]$. In Scenarios I and II, we used Kaplan-Meier weights to account for censoring; in Scenario III, we used both Kaplan-Meier and model-based weights.

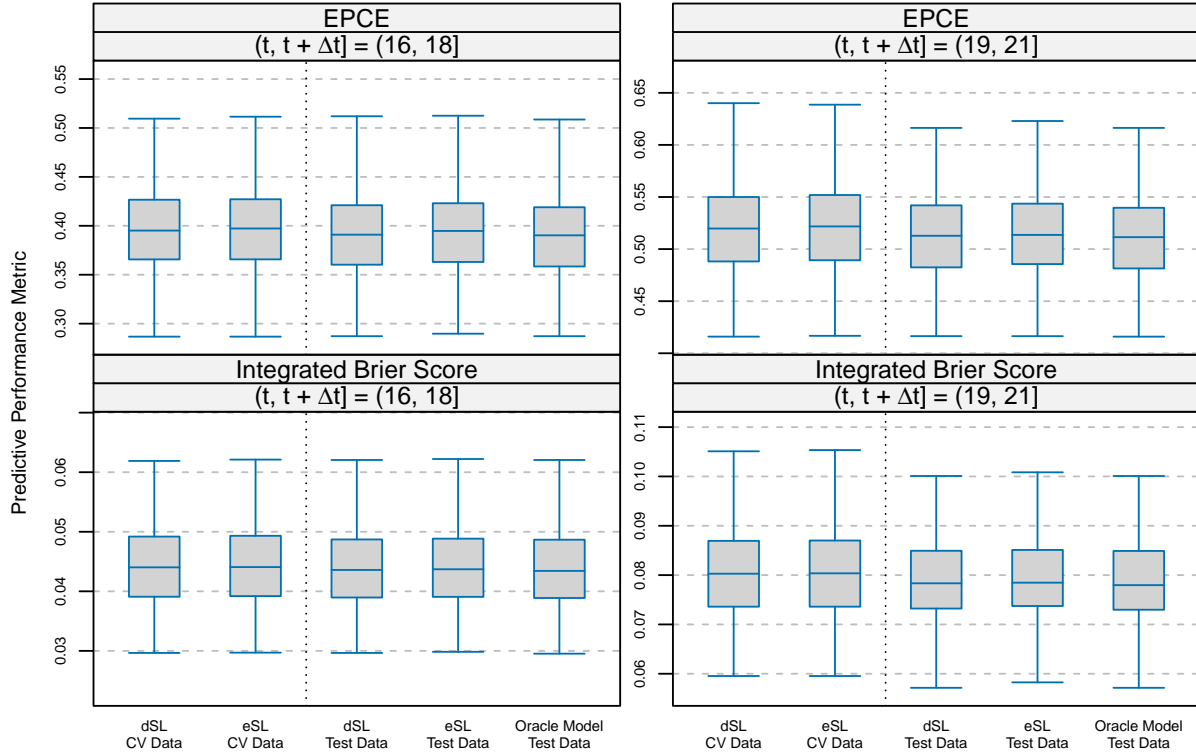


Figure 1: Simulation results for the expected predictive cross-entropy (EPCE) and the integrated Brier score under Scenario I. The left and right panels show the results for the two time intervals $(t, t + \Delta t]$. In each panel, five boxplots are shown summarizing the results over the 250 simulated datasets; the first two show the results of the discrete super learner (dSL) and the ensemble super learner (eSL) from the cross-validation procedure in the training dataset; the last three show the results of dSL, eSL, and the oracle model in the independent testing dataset. Each simulated training and testing dataset contains 750 subjects.

5.2 Results

Figures 1 and 2 show the results for the integrated Brier score and the EPCE under the first two scenarios, respectively. In each figure, the left and right panels show the results for the two time intervals $(16, 18]$ and $(19, 21]$, respectively. The top and bottom panels show the results for the two accuracy metrics. In each panel, five boxplots are depicted summarizing the results over the 250 simulated datasets. The first boxplot shows the results of the corresponding predictive performance metric for the discrete super learner (dSL), i.e.,

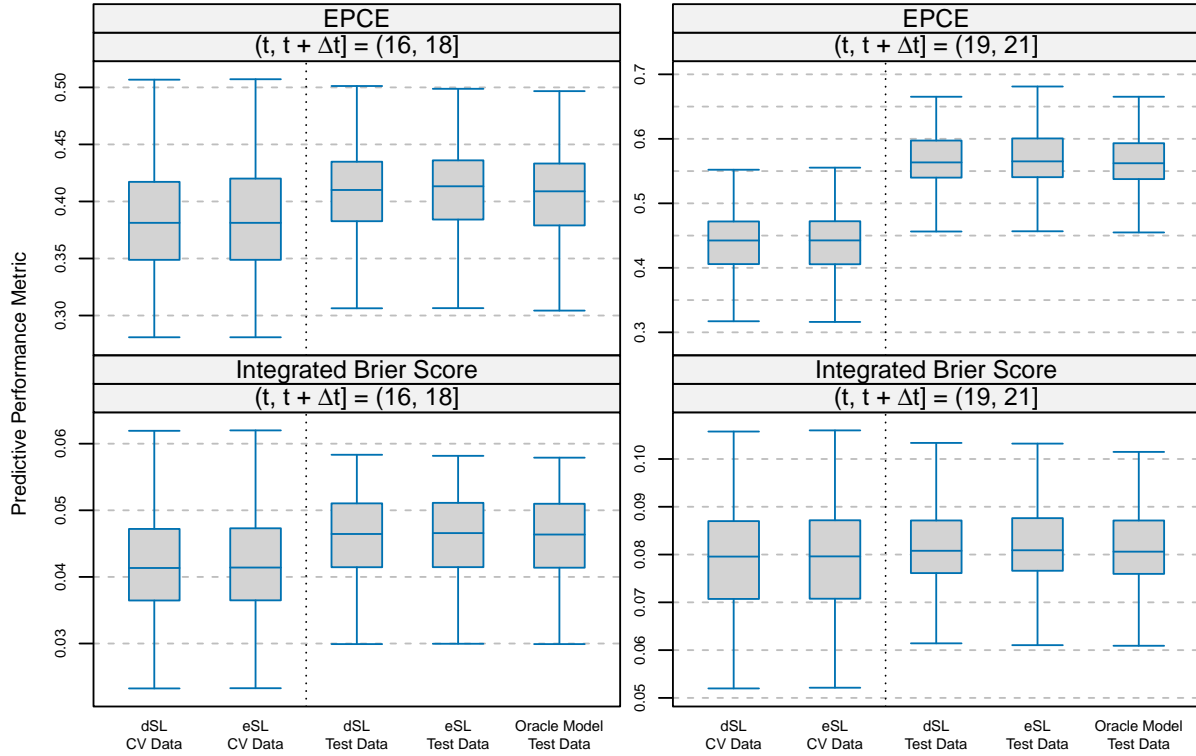


Figure 2: Simulation results for the expected predictive cross-entropy (EPCE) and the integrated Brier score under Scenario II. The left and right panels show the results for the two time intervals $(t, t + \Delta t]$. In each panel, five boxplots are shown summarizing the results over the 250 simulated datasets; the first two show the results of the discrete super learner (dSL) and the ensemble super learner (eSL) from the cross-validation procedure in the training dataset; the last three show the results of dSL, eSL, and the oracle model in the independent testing dataset. Each simulated training and testing dataset contains 750 subjects.

the model that performed the best in the cross-validation procedure applied in the training dataset. The second boxplot corresponds to the result of the ensemble super learner (eSL) in the training dataset using the cross-validated predictions. The third and fourth boxplots show the results under the dSL and eSL, respectively, but are evaluated in the independent testing dataset. The last boxplot shows the results of the Oracle model, i.e., the model with the lowest value for the predictive performance metric in the testing dataset. Figure 3 shows the results for the integrated Brier score under Scenario III. The left and right panels correspond to the model-based and inverse probability of censoring weights to account for the informative censoring. The top and bottom panels show the results for the two time intervals $(19, 21]$ and $(16, 18]$, respectively. In each panel, the same five boxplots are depicted as in Figures 1–2.

Both metrics indicate that the predictive accuracy in the interval $(19, 21]$ is worse than in $(16, 18]$. This is attributed to the fact that more events are observed in the $(16, 18]$ interval than in the $(19, 21]$ one, leading to a better estimate of the underlying baseline hazard function. In the cross-validated training datasets, eSL performs as well as the dSL under both Scenarios I and II. The performance of the dSL and eSL is the same as that of the oracle model in the independent test datasets. Figures 3 and 4 in the supplementary material zoom in on the performance of the dSL and eSL relative to the oracle model in the test datasets. From these figures, we observe that dSL performs slightly better than the eSL. In Scenario II, all metrics perform worse in the test datasets than in the cross-validated training datasets, indicating a greater degree of overfitting. In Scenario I, both metrics perform slightly better in the test dataset than in the cross-validated training ones. Tables 1 and 2 in the supplementary material show the median estimated weight and interquartile range per model, predictive metric and interval for the first two scenarios, respectively. We see that in Scenario I all models receive the same weight for both metrics and intervals. In Scenario II, the weights for the EPCE metric favor the models with the velocity functional form and the nonlinear time trajectories. The weights for IBE in Scenario II do not favor

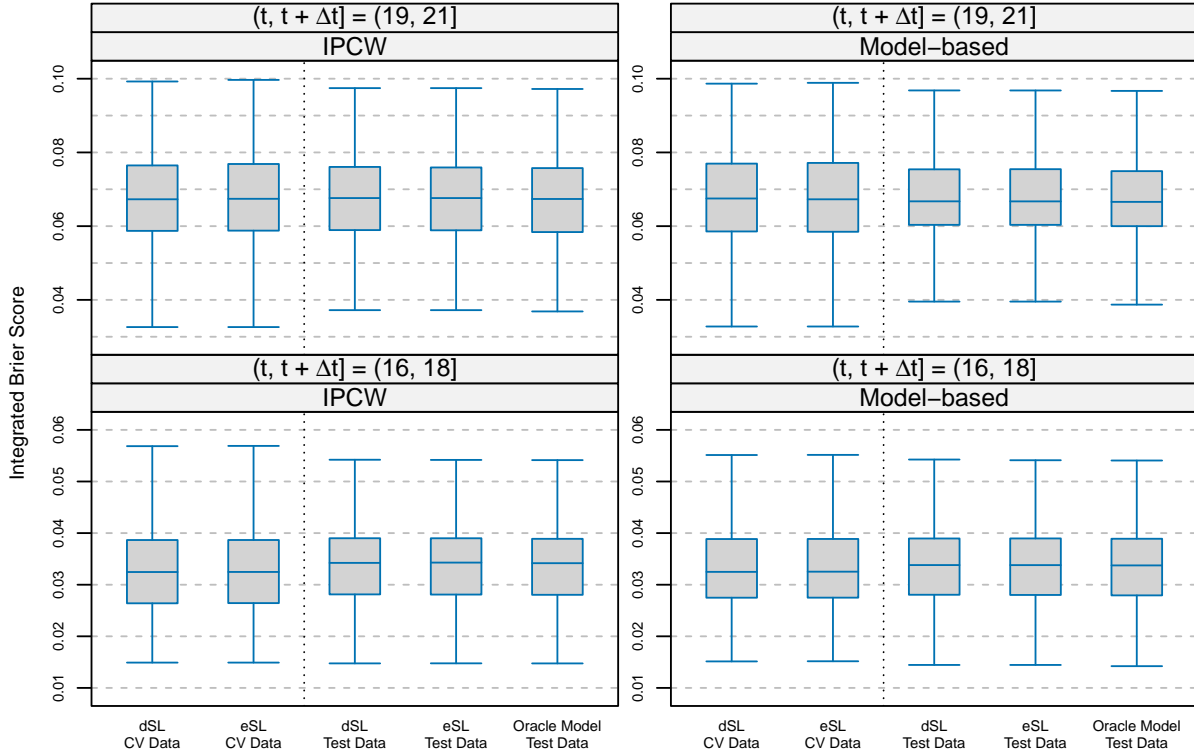


Figure 3: Simulation results for the integrated Brier score under Scenario III. The top and bottom panels show the results for the two time intervals $(t, t + \Delta t]$. The left and right panels show the results using model-based and inverse probability of censoring weights to account for informative censoring. In each panel, five boxplots are shown summarizing the results over the 250 simulated datasets; the first two show the results of the discrete super learner (dSL) and the ensemble super learner (eSL) from the cross-validation procedure in the training dataset; the last three show the results of dSL, eSL, and the oracle model in the independent testing dataset. Each simulated training and testing dataset contains 750 subjects.

any specific model. In Scenario III, we observe small differences between the IPCW and the model-based weights to account for the informative censoring.

6 Discussion

In this paper, we presented an adaptation of the super learning framework for optimizing dynamic predictions from joint models for longitudinal and time-to-event data. We considered the Brier score and the expected predictive cross-entropy as predictive accuracy metrics and compared two super learning versions. Namely, the discrete super learner selects the model with the best cross-validated prediction metric among the candidate models, and the ensemble super learner specifies an optimal convex combination of the predictions from all candidate models. In the University of Michigan Prostatectomy Data, the ensemble super learner performed better than the discrete one, especially when using the expected predictive cross-entropy as an accuracy metric. However, in the simulation study, we observed small differences, and both versions performed as well as the oracle model selector. The suboptimal performance of the super learner for the Brier score metric in the simulation study and the motivating example can be explained by the limited ability of this metric to discern between models (Wilks 2010; Benedetti 2010).

The use of V -fold cross-validation is key for optimizing the performance of super learners. However, this requirement makes SL a computationally challenging task. We utilized parallel computing to mitigate the computational cost in both the analysis of the University of Michigan Prostatectomy Data and the simulation. Another practical aspect of using V -fold cross-validation is the choice of V . For binary outcomes, Phillips et al. (2023) suggested using larger values of V for a smaller effective sample size. In our test simulation runs, we found that smaller values of V produce more stable results for smaller effective sample sizes. This is because in the time-to-event data context, we apply cross-validation at different follow-up times, and we require to have a sufficient number of events in each of these intervals. In this

setting, selecting a larger V would result in time intervals having very few or no events.

The super learning framework we presented here can be augmented with alternative procedures for dynamic predictions; for instance, the landmark approach ([van Houwelingen and Putter 2011](#)) or machine learning procedures, such as deep learning ([Lee et al. 2020](#)). In addition, the SL framework could be extended in settings with competing risks and multi-state processes or recurrent events. However, such extensions require appropriate adaptations of the predictive accuracy metrics.

Funding

The authors thank the NIH CISNET Prostate Award CA253910 for financial support.

Supplementary Material

Supplementary material are available with this paper.

References

- Benedetti, R. (2010). Scoring rules for forecast verification. *Monthly Weather Review* **138**, 203–211.
- Breiman, L. (1996). Stacked regressions. *Machine Learning* **24**, 49–64.
- Commenges, D., Liquef, B., and Proust-Lima, C. (2012). Choice of prognostic estimators in joint models by estimating differences of expected conditional Kullback-Leibler risks. *Biometrics* **68**, 380–387.
- Ferrer, L., Putter, H., and Proust-Lima, C. (2019). Individual dynamic predictions using landmarking and joint modelling: Validation of estimators and robustness assessment. *Statistical Methods in Medical Research* **28**, 3649–3666.

- Hoeting, J., Madigan, D., Raftery, A., and Volinsky, C. (1999). Bayesian model averaging: A tutorial. *Statistical Science* **14**, 382–417.
- Kvamme, H. and Borgan, O. (2023). The Brier score under administrative censoring: Problems and a solution. *Journal of Machine Learning Research* **24**, 1–26.
- Lee, C., Yoon, J., and Schaar, M. (2020). Dynamic-DeepHit: A deep learning approach for dynamic survival analysis with competing risks based on longitudinal data. *IEEE Transactions on Biomedical Engineering* **67**, 122–133.
- Lewandowski, D., Kurowicka, D., and Joe, H. (2009). Generating random correlation matrices based on vines and extended onion method. *Journal of Multivariate Analysis* **100**, 1989–2001.
- Naimi, A. and Balzer, L. (2018). Stacked generalization: An introduction to super learning. *European Journal of Epidemiology* **33**, 459–464.
- Phillips, R., van der Laan, M., Lee, H., and Gruber, S. (2023). Practical considerations for specifying a super learner. *International Journal of Epidemiology* **52**, 1276–1285.
- Rindt, D., Hu, R., Steinsaltz, D., and Sejdinovic, D. (2022). Survival regression with proper scoring rules and monotonic neural networks. In Camps-Valls, G., Ruiz, F., and Valera, I., editors, *Proceedings of the the 25th International Conference on Artificial Intelligence and Statistics (AISTATS) 2022, Valencia, Spain*.
- Rizopoulos, D. (2011). Dynamic predictions and prospective accuracy in joint models for longitudinal and time-to-event data. *Biometrics* **67**, 819–829.
- Rizopoulos, D. (2012). *Joint Models for Longitudinal and Time-to-Event Data, with Applications in R*. Chapman & Hall/CRC, Boca Raton.

- Rizopoulos, D., Hatfield, L., Carlin, B., and Takkenberg, J. (2014). Combining dynamic predictions from joint models for longitudinal and time-to-event data using Bayesian model averaging. *Journal of the American Statistical Association* **109**, 1385–1397.
- Rizopoulos, D., Papageorgiou, G., and Afonso, P. (2023). *JMbayes2: Extended Joint Models for Longitudinal and Time-to-Event Data*. R package version 0.4-5.
- Taylor, J., Park, Y., Ankerst, D., Proust-Lima, C., Williams, S., Kestin, L., Bae, K., Pickles, T., and Sandler, H. (2013). Real-time individual predictions of prostate cancer recurrence using joint models. *Biometrics* **69**, 206–213.
- Taylor, J., Yu, M., and Sandler, H. (2005). Individualized predictions of disease progression following radiation therapy for prostate cancer. *Journal of Clinical Oncology* **23**, 816–825.
- van der Laan, M., Dudoit, S., and van der Vaart, A. (2006). The cross-validated adaptive epsilon-net estimator. *Statistics & Decision* **24**, 373.
- van der Laan, M., Dudoit, S., and van der Vaart, A. (2007). Super learner. *Statistical Applications in Genetics and Molecular Biology* **6**, Article 25.
- van Houwelingen, H. and Putter, H. (2011). *Dynamic Prediction in Clinical Survival Analysis*. Chapman & Hall/CRC, Boca Raton.
- Wilks, D. (2010). Sampling distributions of the Brier score and Brier skill score under serial dependence. *Quarterly Journal of the Royal Meteorological Society* **136**, 2109–2118.